Unsteady flow evolution in swirl injectors with radial entry. II. External excitations

Shanwu Wang[a)] and Vigor Yang
Department of Mechanical and Nuclear Engineering, The Pennsylvania State University, University Park, Pennsylvania 16802

(Received 10 June 2004; accepted 13 January 2005; published online 31 March 2005)

Our previous study on turbulent flows in a gas-turbine swirl injector was extended to explore the effects of externally impressed excitations on the unsteady flow evolution. Three-dimensional large-eddy simulations were conducted to investigate the responses of the injector flowfield by imposing periodical oscillations of the mass flow rate at the entrance over a wide range of frequencies. Results show that the impressed disturbances are decomposed and propagate in two different modes because of their distinct propagating mechanisms in swirl injectors. The flow oscillation in the streamwise direction travels in the form of acoustic wave, whereas the oscillation in the circumferential direction is convected downstream with the local flow velocity. The vortex breakdown is mainly controlled by the dynamics in the core region near the axis, not so much by the excitation in the main flow passage surrounding the central recirculation zone. External excitations only exert minor influences on the mean flow properties due to the broadband characteristics of the injector flow. One exception is in the outer shear-layer region when the forcing frequency matches the intrinsic frequency of vortex shedding, and the mixing process of two counter-rotating swirl flows is considerably enhanced. The dynamic response of the injector flow, however, depends significantly on the forcing frequency in terms of the acoustic admittance and the mass transfer functions. Energy can be transferred among the various structures in the flowfield under external excitations, causing highly nonuniform spatial and temporal distributions of the oscillatory flow properties at the injector exit. The mass transfer function between the injector exit and entrance at the forcing frequency could be substantially greater than unity when the disturbance resonates with the injector flow. The injector essentially acts as an amplifier under this condition.
 [DOI: 10.1063/1.1874932]

I. INTRODUCTION

The present work extends our earlier study on unsteady flow evolution in a gas-turbine swirl injector[1] to investigate its dynamic response to externally impressed excitations. The forcing is obtained by imposing periodical oscillations of mass flow rate at the injector entrance over a broad range of frequencies relevant to the intrinsic flow instabilities in the injector.

The response of a dynamic system can be conveniently examined by exciting the system at discrete sinusoidal frequencies. Considerable efforts have been devoted to studying forced shear layers and jets in the past few decades. Ho and Huerre[2] concluded in their comprehensive review of perturbed free shear layers that monochromatic excitation could suppress broadband background noise and lead to well-organized vortical structures. In addition, single-frequency excitation may considerably delay the appearance of other frequency components observed in shear flows without forcing, a situation commonly known as the frequency-locking phenomenon. Panda and McLaughlin[3] explored the effects of excitations on the flow structures of swirling jets using flow visualization techniques. Weak, irregular, large-scale organized structures under conditions without forcing became energetic and periodic when the jet was excited by acoustic oscillations with discrete frequencies in the upstream region. Cerecedo *et al.*[4] found that for a co-flow jet, external forcing at subharmonic or natural frequencies significantly changes turbulent properties; however, only modest influence was observed when the forcing frequency is twice the nature frequency. They also noted an energy transfer phenomenon between the mean, phase averaging, and random flowfields.

Apte and Yang[5] examined the unsteady flow evolution in a porous-walled chamber with impressed periodic excitations at the exit, which led to an earlier laminar-to-turbulence transition than that in stationary flows. Observations were also made of significant changes in the unsteady flowfield caused by the interactions between turbulent and acoustic motions.

Cohen and Hibshman[6] studied the response of a two-passage swirl injector over a frequency range from 300 to 600 Hz. An electro-pneumatic actuator (Ling driver) was employed to generate a sinusoidally oscillating flow entering the swirler. The acoustic impedance, defined as a transfer function of the fluctuations between the outlet flow velocity and the inlet pressure, was measured as a function of excitation frequency to characterize the injector response. It was found that the velocity near the wall between the two passages was highly sensitive to external forcing for frequencies between 400 and 600 Hz. This phenomenon was attributed to periodic vortex shedding or other velocity-sensitive mecha-

a)Electronic mail: shanwu@psu.edu

nisms. Paschereit and his co-workers[7] investigated the role of coherent structures in a swirl-stabilized combustor using acoustic drivers to modify the boundary condition downstream of the combustor, and highlighted the axisymmetric motion during the unsteady combustion process as the dominant mode. Lieuwen and Neumeier[8] studied the behavior of a premixed swirl-stabilized combustor subject to pressure perturbations in the downstream region. The heat-release fluctuation increases with increasing amplitude of the imposed acoustic oscillation, but levels off when the excitation amplitude exceeds a threshold value. A frequency-lock phenomenon was also noted when the forcing frequency differs the nature frequency of the system.

In contrast to the aforementioned studies, in which significant influences arising from external excitations were observed, only a minor effect was reported by Brereton and his co-workers[9] in their study of the response of a fully developed flat-plate turbulent boundary layer to periodic fluctuations in the downstream region. They concluded that the flow characteristics in boundary layers under conditions with and without free-stream oscillations were equivalent to each other over a wide range of forcing frequencies. This phenomenon may be attributed to the broadband nature of a turbulent boundary layer. Gallaire *et al.*[10] recently conducted an experimental study on the helical modes of free and forced swirling jets. The vortex breakdown was found to be extremely robust, and remained basically unaffected by the azimuthal forcing imposed in the upstream region. Since the vortex breakdown was primarily governed by the dynamics in the core region, external forcing failed to modulate the process.

In spite of extensive studies of forced non-swirling flows, information about forced swirling flows appears to be limited. The present work attempts to study the dynamic response of a swirl injector, motivated by the experiments of Cohen and Hibshman.[6] The study employs a time-resolved, large-eddy-simulation (LES) technique that allows the flowfield to be resolved at a scale sufficient to characterize the injector flow dynamics. The external forcing is implemented by periodically varying the mass flow rate at the injector entrance at discrete frequencies. The paper is arranged as follows. Section II describes the flow condition and data analysis methods. Section III examines the response of the injector flowfield to external forcing. The acoustic admittance and several transfer functions are calculated to characterize the injector dynamics. Finally, a summary is presented in Sec. IV.

II. FLOW CONDITION AND DATA ANALYSIS

In Part I of the current study,[1] vortical flow dynamics in a gas-turbine swirl injector comprising three passages was investigated using large-eddy simulations. Air enters the injector through three sets of radial-entry, counter-rotating swirl vanes, and then exits to the ambient room conditions. Both high and low swirl-number cases were treated. Figure 1 shows a snapshot of the axial-vorticity field for the high swirl-number ($S=0.5$) case. The large flow structure in the region downstream of the centerbody indicates the presence

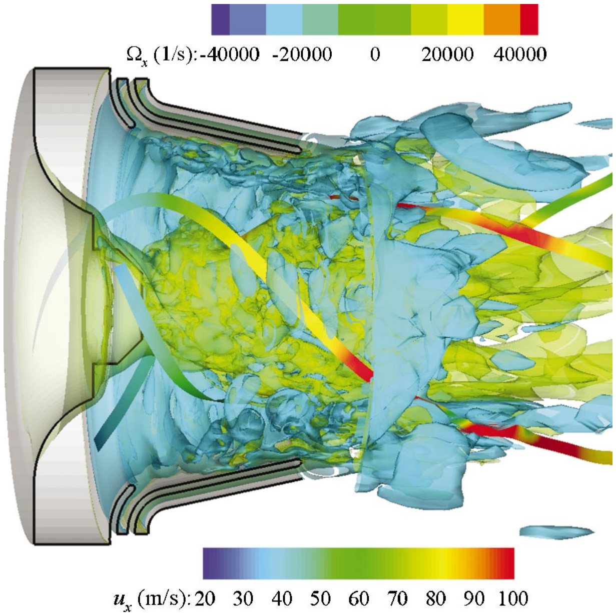

FIG. 1. (Color). Iso-surface of axial vorticity at $\Omega_x=-2000$ and 2000 1/s for high swirl number ($S=0.5$) case without forcing.

of a central toroidal recirculation zone (CTRZ) arising from vortex breakdown. The flow characteristic frequency in this region is 4.0 kHz. A three-dimensional proper orthogonal decomposition (POD) analysis was conducted for the pressure field to study the dominant mechanisms in the complex flow motion. The mode shape corresponding to the frequency of 4.0 kHz, shown in Fig. 2, clearly reveals a precessing vortex motion along the boundary of the central recirculating flow. A detailed description of the POD analysis can be found in Part I of this study. The frequency spectrum of the velocity field indicates that the pressure fluctuation is tightly coupled with the radial velocity instead of the other velocity components near the boundary of the central recirculation zone. Meanwhile, a strong shear layer originating from the rim of the first guide vane induces organized vortex shedding along the inner side of the second guide vane at a frequency of around 13 kHz. These two distinct flow patterns

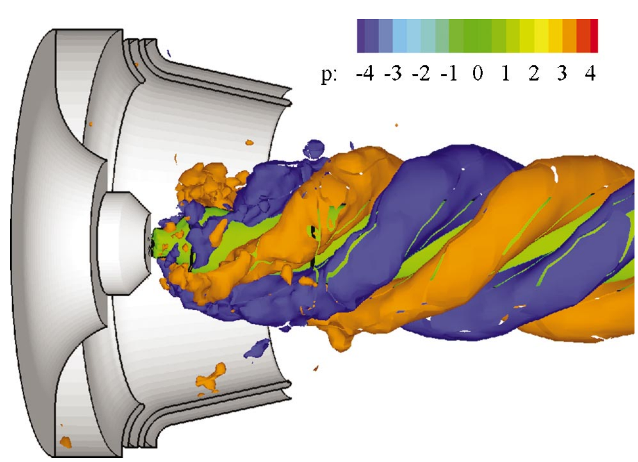

FIG. 2. (Color). POD mode shape of pressure field showing existence of precessing vortex ($f=4.0$ kHz).

interact with each other near the injector exit. The specific coupling depends strongly on the swirl number, and may involve an array of frequencies related to the instability mechanisms in various flow regions. The flowfield in the injector can be regarded as a distributed dynamic system with a wide range of well-defined intrinsic frequencies.

The swirl injector examined in Part I of this study is also investigated in the present work. The theoretical formulation and numerical method are identical, except for the modification of the inlet boundary condition to accommodate the modulation of the mass flow rate. The flow condition corresponds to the high swirl-number case in Part I. The Reynolds number, Re, is 2×10^5 and the angles of the three counter-rotating radial swirl vanes are $S_1=45°$, $S_2=-60°$, and $S_3=70°$. A total of two-million grid points are used in this three-dimensional simulation, and the physical time step employed is $\Delta t=5\times 10^{-5}$ ms. The calculation is first performed over an extended time period until the flowfield reaches its stationary state. Data are then collected for 20 ms (more than 30 flow-through times) to obtain statistically meaningful turbulence properties for each case.

Periodical oscillations of the mass flow rate, $\dot{m}$, are enforced at the injector entrance, similar to the experiment conducted by Cohen and Hibshman,[6]

$$\dot{m} = \dot{m}_0[1 + \alpha \sin(2\pi f_F t)], \tag{1}$$

where $\dot{m}_0$ and f_F denote the mean mass flow rate and the forcing frequency, respectively. The amplitude of the oscillation, α, is fixed at 10%. The forcing frequency covers a range from 400 through 13 000 Hz, due to the broadband nature of the injector flow dynamics.[1] Turbulence with an intensity of 8% of the mean flow quantity is provided by superimposing broadband noise with a Gaussian distribution.

As a consequence of impressed periodic oscillations, the flowfield contains contributions from both well-organized (deterministic) motions and random (stochastic) turbulent fluctuations. For incompressible flows, the triple decomposition method developed by Hussain and Reynolds[11] can be employed to analyze the flow motion. Each variable $\Im$ is decomposed into three parts as follows:

$$\Im(\mathbf{x},t) = \overline{\Im}(\mathbf{x}) + \Im^a(\mathbf{x},t) + \Im^t(\mathbf{x},t), \tag{2}$$

where $\overline{\Im}, \Im^a$, and $\Im^t$ denote long-time averaged, phase averaged, and turbulent components, respectively. The long-time averaged quantity $\overline{\Im}$ is defined as

$$\overline{\Im}(\mathbf{x}) = \lim_{N\to\infty} \frac{1}{N} \sum_{n=0}^{N-1} \Im(\mathbf{x}, t_0 + n\Delta t). \tag{3}$$

The deterministic periodic motion can be obtained using phase averaging based on the given forcing period, τ, i.e.,

$$\langle \Im(\mathbf{x},t)\rangle = \overline{\Im}(\mathbf{x}) + \Im^a(\mathbf{x},t) = \lim_{N\to\infty} \frac{1}{N} \sum_{n=0}^{N-1} \Im(\mathbf{x}, t_0 + n\tau), \tag{4}$$

where $\tau=1/f_F$ and $\tau \gg \Delta t$.

Apte and Yang[5] and Huang[12] further extended this technique to include compressibility effects using the density-weighted (Favre-averaged) time-averaging and phase-averaging methods given below:

$$\Im(\mathbf{x},t) = \overleftrightarrow{\Im}(\mathbf{x}) + \Im^{\overleftrightarrow{a}}(\mathbf{x},t) + \Im^{\overleftrightarrow{t}}(\mathbf{x},t), \tag{5}$$

where the density-weighted long-time averaged $\overleftrightarrow{\Im}$ and phase averaged $\Im^{\overleftrightarrow{a}}$ are defined as

$$\overleftrightarrow{\Im}(\mathbf{x}) = \overline{\rho(\mathbf{x},t)\Im(\mathbf{x},t)}/\overline{\rho}(\mathbf{x}), \tag{6}$$

$$\overleftrightarrow{\Im}(\mathbf{x}) + \Im^{\overleftrightarrow{a}}(\mathbf{x},t) = \langle \rho(\mathbf{x},t)\Im(\mathbf{x},t)\rangle / \langle \rho(\mathbf{x},t)\rangle. \tag{7}$$

Evaluation of the phase average in Eq. (7) requires calculation and storage of an avalanche of data to achieve statistically consistent and meaningful results. To bypass this computational difficulty, a windowed Fourier transform is normally used to extract the deterministic motion from the original time-trace data by choosing the Fourier component at the frequency of concern.

Substitution of Eq. (5) into the momentum equations and application of the intrinsic properties of the density-weighted triple decomposition yields the following long-time averaged transport equations for the kinetic energy of the mean, periodic, and turbulent flowfields.[5,12]

Kinetic energy of mean flowfield:

$$\begin{aligned}\frac{\partial}{\partial x_j}\left(\rho \overleftrightarrow{u}_j \frac{\overleftrightarrow{u}_i\overleftrightarrow{u}_i}{2}\right) = {} & \overline{\rho u_i^{\overleftrightarrow{a}} u_j^{\overleftrightarrow{a}}}\frac{\partial \overleftrightarrow{u}_i}{\partial x_j} + \overline{\rho u_i^{\overleftrightarrow{t}} u_j^{\overleftrightarrow{t}}}\frac{\partial \overleftrightarrow{u}_i}{\partial x_j} - \frac{\partial}{\partial x_j}[\overleftrightarrow{u}_i(\overline{\rho u_i^{\overleftrightarrow{a}} u_j^{\overleftrightarrow{a}}} \\ & + \overline{\rho u_i^{\overleftrightarrow{t}} u_j^{\overleftrightarrow{t}}} + \overline{p}\delta_{ij} - \overline{\sigma}_{ij})] \\ & - \overline{\sigma}_{ij}\frac{\partial \overleftrightarrow{u}_i}{\partial x_j} + \overline{p}\frac{\partial \overleftrightarrow{u}_i}{\partial x_i}.\end{aligned} \tag{8}$$

Kinetic energy of periodic flowfield:

$$\begin{aligned}& \frac{\partial}{\partial x_j}\left(\overline{\rho}\overleftrightarrow{u}_j \overline{\frac{u_i^{\overleftrightarrow{a}} u_i^{\overleftrightarrow{a}}}{2}}\right) + \frac{\partial}{\partial x_j}\overline{\rho u_j^{\overleftrightarrow{a}} \frac{u_i^{\overleftrightarrow{a}} u_i^{\overleftrightarrow{a}}}{2}} \\ & \quad = - \overline{\rho u_i^{\overleftrightarrow{a}} u_j^{\overleftrightarrow{a}}}\frac{\partial \overleftrightarrow{u}_i}{\partial x_j} + \overline{(\rho u_i^{\overleftrightarrow{t}} u_j^{\overleftrightarrow{t}})^a \frac{\partial u_i^{\overleftrightarrow{a}}}{\partial x_j}} - \frac{\partial}{\partial x_j} \\ & \qquad \times \overline{u_i^{\overleftrightarrow{a}}[(\rho u_i^{\overleftrightarrow{t}} u_j^{\overleftrightarrow{t}})^a + p^a\delta_{ij} - \sigma_{ij}^a]} - \overline{\sigma_{ij}^a \frac{\partial u_i^{\overleftrightarrow{a}}}{\partial x_j}} \\ & \qquad - \overline{p^a \frac{\partial u_i^{\overleftrightarrow{a}}}{\partial x_i}} + \overline{u_i^{\overleftrightarrow{a}}}\frac{\partial \overline{\rho u_i^{\overleftrightarrow{a}} u_j^{\overleftrightarrow{a}}}}{\partial x_j} - \frac{\overline{u_i^{\overleftrightarrow{a}} \rho^a \aleph_{\overleftrightarrow{u},i}}}{\overline{\rho}}.\end{aligned} \tag{9}$$

Kinetic energy of turbulent flowfield:

$$\frac{\partial}{\partial x_j}\left(\overline{\rho}\overleftrightarrow{u}_j\frac{\overline{\overleftrightarrow{u}_i^t\overleftrightarrow{u}_i^t}}{2}\right)+\frac{\partial}{\partial x_j}\overline{\rho\overleftrightarrow{u}_j^a\frac{\overleftrightarrow{u}_i^t\overleftrightarrow{u}_i^t}{2}}+\frac{\partial}{\partial x_j}\overline{\rho\overleftrightarrow{u}_j^t\frac{\overleftrightarrow{u}_i^t\overleftrightarrow{u}_i^t}{2}}$$
$$=-\overline{\rho\overleftrightarrow{u}_i^t\overleftrightarrow{u}_j^t}\frac{\partial\overleftrightarrow{u}_i}{\partial x_j}-\overline{(\rho\overleftrightarrow{u}_i^t\overleftrightarrow{u}_j^t)^a\frac{\partial\overleftrightarrow{u}_i^a}{\partial x_j}}-\overline{\rho\overleftrightarrow{u}_i^t\overleftrightarrow{u}_j^t}\frac{\partial\overline{\overleftrightarrow{u}_i^a}}{\partial x_j}$$
$$-\overline{(\rho\overleftrightarrow{u}_i^t\overleftrightarrow{u}_j^t)^t\frac{\partial\overleftrightarrow{u}_i^a}{\partial x_j}}+\frac{\partial}{\partial x_j}\overline{\overleftrightarrow{u}_i^t(\langle\rho\overleftrightarrow{u}_i^t\overleftrightarrow{u}_j^t\rangle+p^t\delta_{ij}-\sigma_{ij}^t)}$$
$$-\overline{\langle\rho\overleftrightarrow{u}_i^t\overleftrightarrow{u}_j^t\rangle\frac{\partial\overleftrightarrow{u}_i^t}{\partial x_j}}-\overline{p^t\frac{\partial\overleftrightarrow{u}_i^t}{\partial x_i}}-\overline{\sigma_{ij}^t\frac{\partial\overleftrightarrow{u}_i^t}{\partial x_j}}-\overline{\frac{\overleftrightarrow{u}_i^t\rho^t\aleph_{\langle u\rangle,i}}{\langle\rho\rangle}}, \qquad (10)$$

where repeated subscripts, i and j, imply summation, and

$$\aleph_{\overleftrightarrow{u},i}=-\frac{\partial\overline{\rho\overleftrightarrow{u}_i^a\overleftrightarrow{u}_j^a}}{\partial x_j}-\frac{\partial\overline{\rho\overleftrightarrow{u}_i^t\overleftrightarrow{u}_j^t}}{\partial x_j}-\frac{\partial\overline{p}}{\partial x_i}+\frac{\partial\overline{\sigma}_{ij}}{\partial x_j}=\frac{\partial(\overline{\rho}\overleftrightarrow{u}_i\overleftrightarrow{u}_j)}{\partial x_j}, \qquad (11)$$

$$\aleph_{\langle u\rangle,i}=-\frac{\partial\langle\rho\overleftrightarrow{u}_i^t\overleftrightarrow{u}_j^t\rangle}{\partial x_j}-\frac{\partial\langle p\rangle}{\partial x_i}+\frac{\partial\langle\sigma_{ij}\rangle}{\partial x_j}$$
$$=\frac{\partial\langle\rho(\overleftrightarrow{u}_i+\overleftrightarrow{u}_i^a)\rangle}{\partial t}+\frac{\partial\langle\rho\rangle(\overleftrightarrow{u}_i+\overleftrightarrow{u}_i^a)(\overleftrightarrow{u}_j+\overleftrightarrow{u}_j^a)}{\partial x_j}. \qquad (12)$$

Here $\aleph_{\overleftrightarrow{u},i}$ and $\aleph_{\langle u\rangle,i}$ represent the net forces on the flow element in the long-time averaged and phase averaged flowfields, respectively.

In the kinetic energy equation of the mean flowfield, Eq. (8), the term $\overline{\rho\overleftrightarrow{u}_i^t\overleftrightarrow{u}_j^t}\partial\overleftrightarrow{u}_i/\partial x_j$ is responsible for energy transfer from the mean flow to turbulence, and the term $\overline{\rho\overleftrightarrow{u}_i^a\overleftrightarrow{u}_j^a}\partial\overleftrightarrow{u}_i/\partial x_j$ accounts for energy transfer from the mean flowfield to organized flow oscillations resulting from periodic oscillation. In the kinetic energy equation of the periodic flowfield, Eq. (9), the energy transferred from the organized flow to turbulence is accomplished by the $\overline{(\rho\overleftrightarrow{u}_i^t\overleftrightarrow{u}_j^t)^a\partial\overleftrightarrow{u}_i^a/\partial x_j}$ term. Obviously, the introduction of organized flow oscillations provides an additional pathway to transfer energy from the mean flowfield to turbulent motion in comparison with stationary flow conditions. The viscous dissipation terms in the three kinetic energy equations, i.e., $-\overline{\sigma}_{ij}\partial\overleftrightarrow{u}_i/\partial x_j, -\overline{\sigma_{ij}^a\partial\overleftrightarrow{u}_i^a/\partial x_j}$, and $-\overline{\sigma_{ij}^t\partial\overleftrightarrow{u}_i^t/\partial x_j}$, and the volume dilatation terms, i.e., $\overline{p}\partial\overleftrightarrow{u}_i/\partial x_i, \overline{p^a\partial\overleftrightarrow{u}_i^a/\partial x_i}$, and $\overline{p^t\partial\overleftrightarrow{u}_i^t/\partial x_i}$, account for the transfer between the kinetic and internal energy. All terms including p^a, p^t, or $\overleftrightarrow{u}_i^a$ result from compressibility effects.

III. RESULTS AND DISCUSSION

The vortical and acoustic fields in the injector can be globally characterized by two frequencies, f_v and f_a, measuring the convective and acoustic motions, respectively. The former can be estimated by the mean-flow residence time, and has a value of 1.7 kHz. The latter is obtained based on the time required for downstream acoustic wave to travel through the injector, and has a value of 11 kHz. The phase difference of the traveling acoustic wave between the entrance and the exit of the injector, θ, is

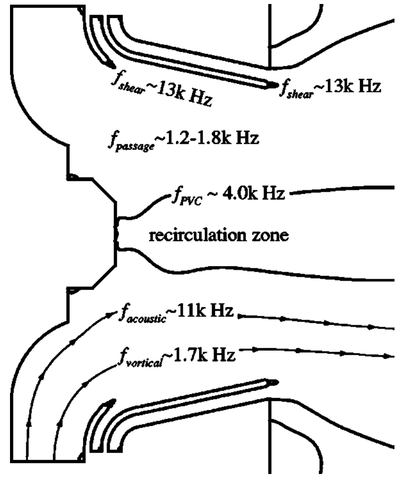

FIG. 3. Characteristic frequencies in the injector.

$$\theta\approx 2\pi L/l_F=2\pi f_F/f_a, \qquad (13)$$

where L is the length of the main flow passage and l_F the acoustic wavelength at the forcing frequency. Figure 3 shows the characteristic frequencies in different regions of the flowfield, obtained from the spectral analysis of the flow motion in Part I of the study.[1]

A. Instantaneous flow structures

Figure 4 shows the snapshots of the fluctuating vorticity magnitude fields, $|\Omega'|$, obtained by subtracting the long-time averaged quantity from its instantaneous value, at various forcing frequencies. When the frequency is higher than f_v, well-defined vortical structures are observed in the forward section of the injector. These waves, generated by the flow oscillations at the entrance, are convected downstream with the local flow velocity. The wavelength is inversely proportional to the forcing frequency, and shortens in the middle region of the injector due to the flow turning effect, i.e., the flow direction turns in this region and the velocity component perpendicular to the wave front decreases. The intensive turbulent fluctuations downstream of the centerbody overshadow the organized vortical waves, which are eventually damped out by turbulent diffusion and viscous dissipation. When the forcing frequency is less than f_v, it is difficult to clearly observe organized vortical waves inside the injector because of the long vortical wavelengths associated with the low-frequency oscillations.

Figure 5 shows snapshots of the fluctuating velocity and pressure fields under external forcing with a frequency of 13 000 Hz. This case was chosen because of the presence of a well-established vortical wave, which helps identify the disturbance propagation mechanisms. The vortical wave is mainly aligned with the fluctuating azimuthal velocity, whereas the acoustic wave is most closely related to the pressure oscillation. The imposed excitation at the injector entrance can be decomposed into two components in the azimuthal and radial directions. The former generates a vortical wave due to the shear stress resulting from the flow oscillation in the azimuthal direction, and its dynamics are gov-

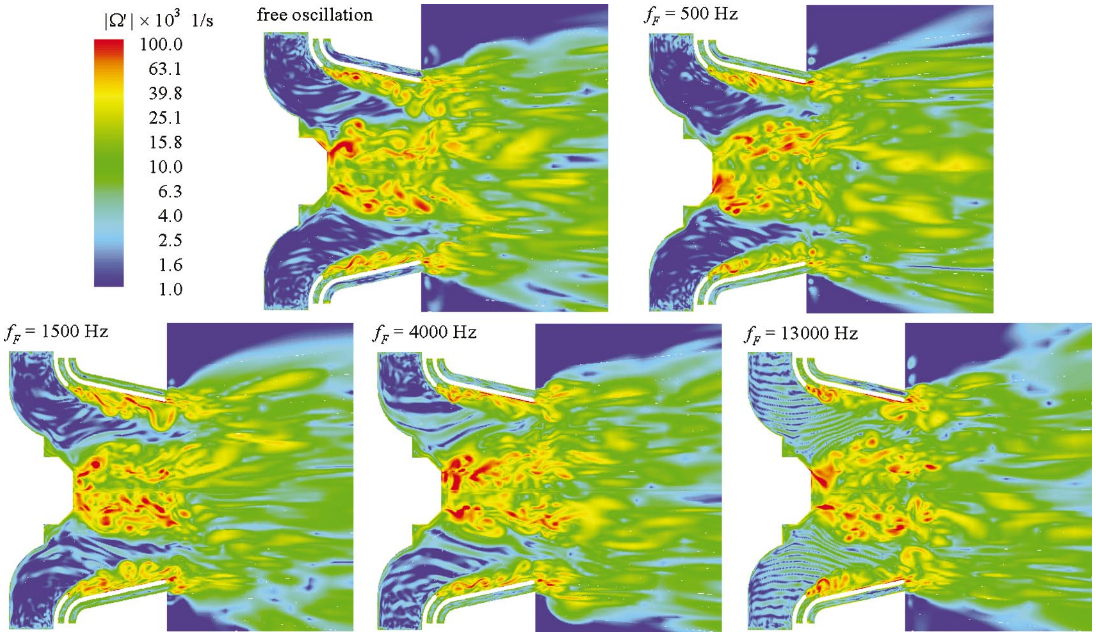

FIG. 4. (Color). Snapshots of fluctuating vorticity magnitude field on a longitudinal cross section under conditions with and without forcing. Contour levels between 10^3 and 10^5 1/s with exponential distribution.

erned by the conservation of angular momentum. The latter produces an irrotational, traveling acoustic wave, and can be characterized by the pressure and streamwise-velocity fluctuations through mass conservation.

To further clarify the wave propagation mechanisms, the fluctuating velocity components in various regions of the injector are investigated. Figure 6 shows the temporal variations of the velocity fluctuations in the streamwise and azimuthal directions at three different locations along the streamline originating from the middle point of the entrance. These measurement points are all in the forward section of the injector, and the corresponding distances from the entrance are 0, 5.9, and 12.2 mm, respectively. Both the streamwise and azimuthal velocity fluctuations increase when the fluid particles travel downstream, due to the conservation of mass and angular momentum, respectively. The traces are

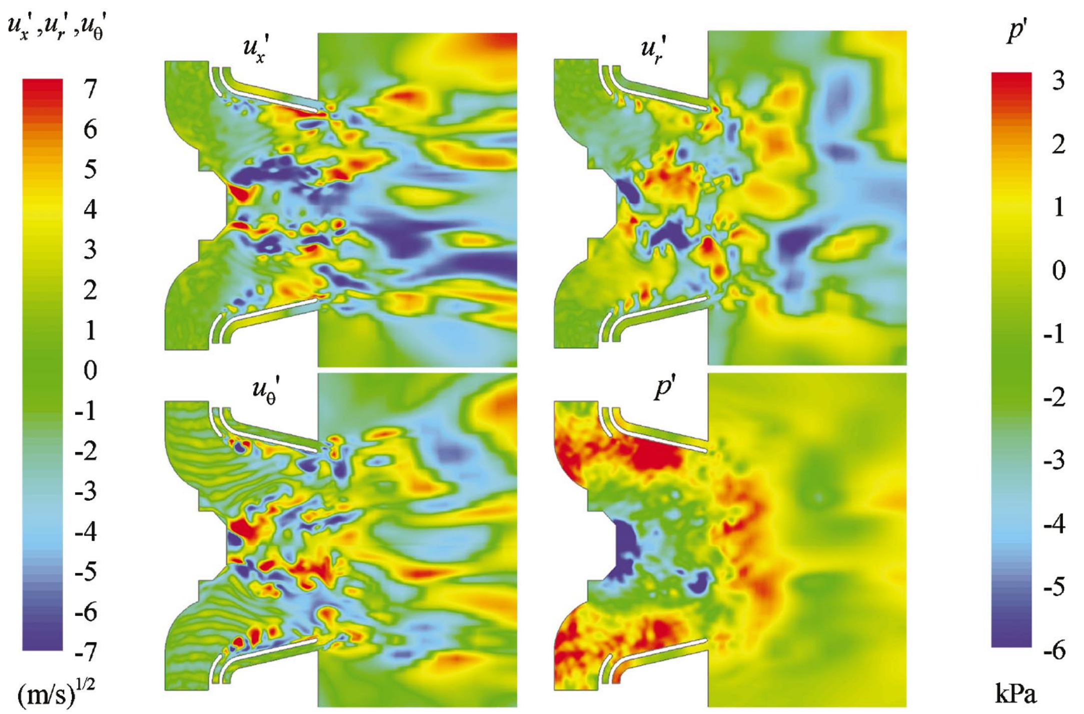

FIG. 5. (Color). Snapshots of velocity and pressure fluctuations at forcing frequency of $f_F = 13\,000$ Hz. Velocity contour levels between −49 and 49 m/s with increment of $0.2\sqrt{\text{m/s}}$ in square root of velocity magnitude; pressure contour levels between −6 and 3 kPa with increment of 0.1 kPa.

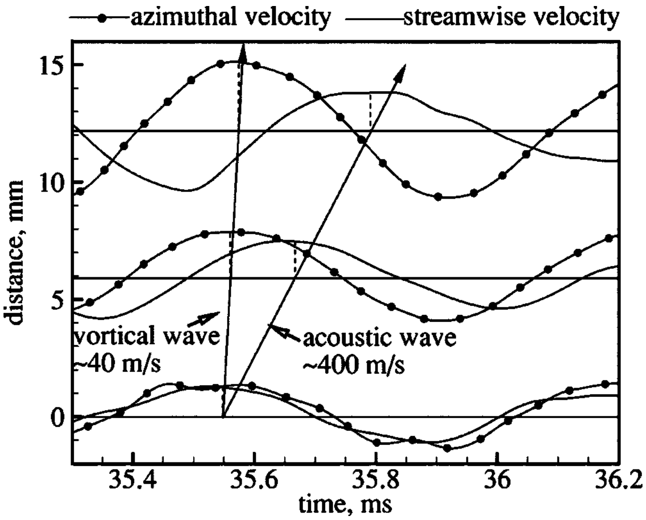

FIG. 6. Fluctuations of streamwise and azimuthal velocities at three different locations along the streamline originating from the middle point of the entrance.

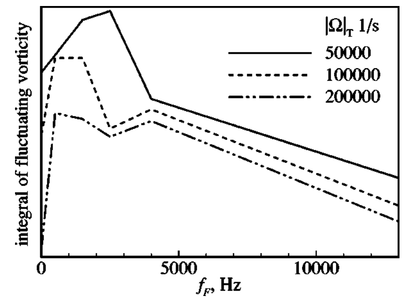

FIG. 7. Integral of vorticity fluctuation in regions with instantaneous vorticity magnitude greater than $|\Omega|_T$ over entire injector flowfield.

smoothed by filtering out the background turbulence. Of particular interest is the propagation of the streamwise disturbance in the form of an acoustic wave with its phase speed equal to the local acoustic wave propagation speed. The flow disturbance in the azimuthal direction, on the other hand, travels in the form of a convective/vortical wave, with its phase speed equal to the local flow velocity. The large disparity between the two phase speeds indicates that the streamwise disturbance arrives in the downstream region much earlier than its azimuthal counterpart. This phenomenon of decomposed-oscillations is analogous to the wave propagation during an earthquake: the vertical oscillation is always detected earlier than the horizontal counterpart at the surface because of the higher propagation speed of the former.

The decoupling between the two velocity oscillations is significant in that the development of the oscillating flowfields in different spatial directions may be quite distinct. Because the fluctuations have the same frequency but different speeds, the vortical wavelength is smaller than its acoustic counterpart by almost one order of magnitude in the present study. Considering the injector dimension and forcing frequency under consideration, the wavelength of the organized vortical motion is closer to the large scales in various regions of the injector, which are less than the characteristic length of the main flow passage. Since interactions between flow motions with similar scales are generally stronger than those with highly disparate scales, a vortical wave with a frequency higher than f_v (i.e., its wavelength less than the flow-passage length) exerts more significant influence on the energy transfer process involving different scales.

As implied in Eqs. (8)–(10), the impressed periodic forcing provides an additional channel to transfer energy between the mean and turbulent flowfields through organized motion. This energy redistribution process is manifested by the presence of vorticity pockets in the flowfield, in which the fluctuating vorticity is greater than a prespecified threshold value, $|\Omega|_T$. Figure 4 shows that those pockets with intensive vorticity fluctuation are enhanced at low forcing frequencies (e.g., 500 and 1500 Hz), but suppressed at high forcing frequencies (e.g., 4000 and 13 000 Hz). To quantify this phenomenon, the fluctuating vorticity within those pockets with their instantaneous magnitude greater than $|\Omega|_T$ is integrated over the entire flowfield. The results for three different threshold values are presented in Fig. 7. The low-frequency forcing promotes flow fluctuation through the excitation of the vortical wave at the entrance. The situation, however, is qualitatively different when the forcing frequency is greater than the injector characteristic frequency for vortical motion (i.e., $f_v = 1.7$ kHz). The corresponding organized short-wavelength motion tends to suppress the development of high-intensity flow oscillation because of its strong shear force. Furthermore, the viscous damping effect increases with the wavelength decrement, and consequently dissipates flow fluctuations more effectively. When the threshold increases, the frequency at which the integral achieves the maximum shifts to the low-frequency regime. The vorticity pockets filtered with a higher threshold represent more intensive vorticity fluctuations, which are normally associated with larger flow structures and are more susceptible to a lower frequency oscillation. In other words, the vorticity integral starts to fall earlier, i.e., at a lower forcing frequency.

The variation of the vorticity pockets against the forcing frequency demonstrates that periodic oscillation plays an important role in the energy transfer, as explained theoretically in Eqs. (8)–(10). In addition to the conventional energy transfer mechanism between the mean and turbulent flowfields, $\overline{\rho \overleftrightarrow{u}_i^t \overleftrightarrow{u}_j^t}\,\partial \vec{\bar{u}}_i/\partial x_j$, a new term, $\overline{\rho \overleftrightarrow{u}_i^a \overleftrightarrow{u}_j^a}\,\partial \vec{\bar{u}}_i/\partial x_j$, provides another channel for energy transfer between the mean and periodic flowfields. This mechanism is finally connected with the turbulent flowfield with the term $\overline{(\rho \overleftrightarrow{u}_i^t \overleftrightarrow{u}_j^t)^a\,\partial u_i^a/\partial x_j}$. It is clear that the additional path is highly dependent on the frequency of the periodic oscillation. When the forcing frequency increases, the length scales of the periodic motions arising from the external excitations inevitably decrease. The gradients of the phase-averaged components (e.g., $\partial \overleftrightarrow{u}_i^a/\partial x_j$) increase and subsequently improve the energy transfer process. For the same reason, the viscous dissipation term resulting from the periodic oscillation, $-\overline{\sigma_{ij}^a\,\partial \overleftrightarrow{u}_i^a/\partial x_j}$, rises accordingly. Thus, more energy is drawn from the mean to the periodic flowfield in order to satisfy the energy balance de-

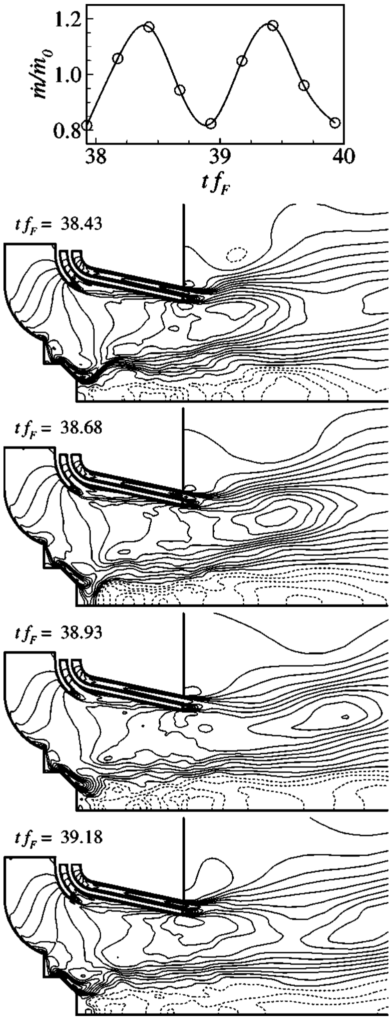

FIG. 8. Time evolution of axial velocity field within one cycle of oscillation with forcing frequency of 1500 Hz, spatially averaged in azimuthal direction. Contour levels between −50 and 100 m/s with increment of 6 m/s. Solid lines: positive values; dashed lines: negative values.

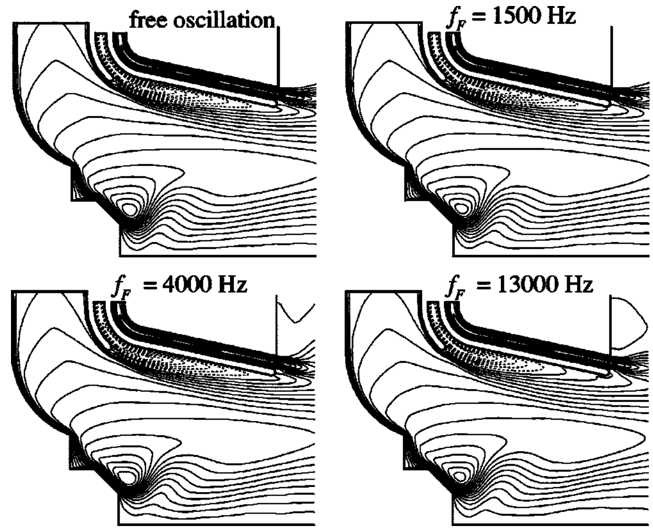

FIG. 9. Effect of forcing frequency on long-time averaged azimuthal velocity field. Contour levels between −90 and 150 m/s with increment of 10 m/s. Solid lines: positive values; dashed lines: negative values.

scribed by Eq. (9), although the process may become indiscernible under low-amplitude forcing. In general, the kinetic energy associated with periodic motion decreases with increasing forcing frequency.

Figure 8 shows the evolution of the instantaneous axial velocity field, which is spatially averaged in the azimuthal direction, within one cycle of oscillation at a forcing frequency of 1500 Hz. Also included is the time trace of the mass flow rate at the injector exit, obtained by filtering out turbulent fluctuations. When the mass flow rate achieves the maximum at $tf_F = 38.43$, a ring structure with strong positive velocity appears in the downstream region of the second guide vane, where the mean axial flow velocity also reaches its maximum. The ring structure then sheds downstream while the mass flow rate decreases. A new one is produced when the mass flow rate increases in a new cycle. The strong flow oscillation in this region can potentially influence the atomization process of the liquid film accumulated on the surface of the second guide vane. This evolution pattern, however, cannot be observed at the other forcing frequencies. The discrepancy may be attributed to the fact that 1500 Hz is closer to the characteristic frequency of flow convection, f_v, than the others studied in the present work. The flow tends to resonate with the external excitation at this frequency in the streamwise direction.

B. Mean flow properties

Figure 9 shows the long-time averaged azimuthal velocity fields at $f_F = 1500$, 4000, and 13 000 Hz. No discernible difference is observed between the flows with and without external excitations except in the region where the counter-rotating flows through the S_1 and S_2 swirlers merge at $f_F = 13\,000$ Hz. The mixing region can be characterized by the line of zero azimuthal velocity, which shrinks by almost half at this forcing frequency. The impressed oscillation resonates with the local shear-layer instability (i.e., 13 000 Hz)[1] when the two frequencies match each other, and even causes the reversal of the azimuthal flow direction. The effect of external forcing on flow development can be further examined in Fig. 10, showing snapshots of the iso-surfaces of the azimuthal velocities at $u_\theta = -2$ and 2 m/s in the azimuthal phase space ($\theta = 0°–360°$). The flowfield exhibits a helical structure originating from the trailing edge of the first guide vane under conditions without external forcing. The coherent structure, however, is destroyed by the impressed axisymmetric disturbance at the injector entrance, and breaks into small bulbs. As discussed in Part I of the present study, two mechanisms, in addition to the external forcing, contribute to this phenomenon: the Kelvin–Helmholtz instability in the azimuthal direction and centrifugal instability. Both of them strongly depend on the swirl number. The ensuing enhancement of flow instability in the azimuthal direction considerably enhances local turbulent mixing. The same phenomenon is observed in the turbulent kinetic energy field. Figure 11 shows the effect of external forcing on turbulence properties. Strong flow resonance occurs at $f_F = 13\,000$ Hz, and consequently leads to a substantial increase in turbulent kinetic energy in the downstream regions of the two guide vanes.

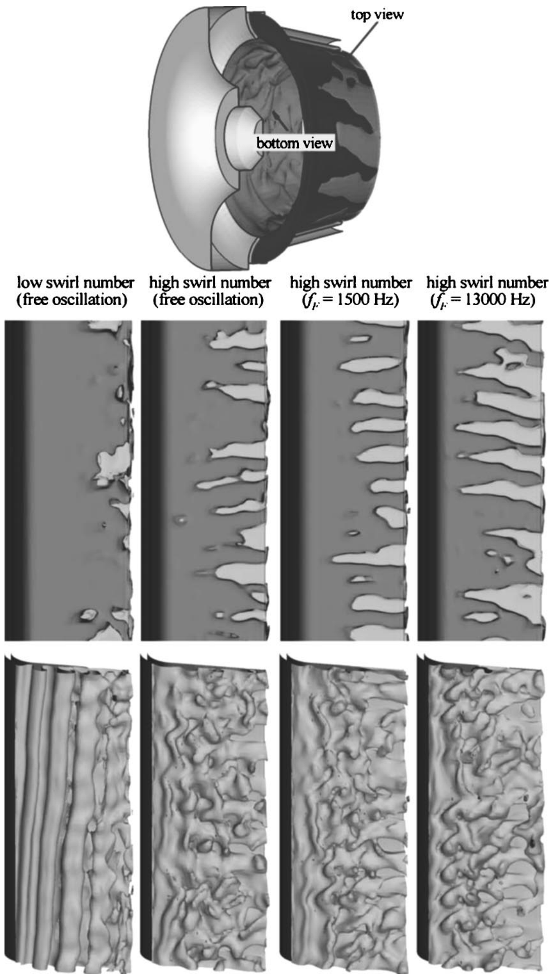

FIG. 10. Snapshots of iso-surfaces of azimuthal velocities at $u_\theta=-2$ and 2 m/s in azimuthal phase space ($\theta=0°-360°$) in shear layer originating from trailing edge of first guide vane. Upper panel: top view; lower: bottom view.

It should be noted that in an operational injector, liquid fuel injected from the centerbody impinges onto the inner surface of the second guide vane and forms a liquid film, which is then atomized to a spray of fine droplets by the local shear flow near the rim of the second guide vane. The potential influence of external forcing on the breakup of the liquid film appears in the two conflicting areas. On the one hand, the strong fluctuation in the azimuthal direction promotes the development of an instability wave on the fuel filming surface and the subsequent atomization process.[13] On the other hand, as shown in Fig. 9, the external forcing may significantly modify the mean azimuthal velocity field near the fuel filming surface, especially when the forcing frequency approaches the shear-layer characteristic frequency (i.e., 13 000 Hz). The flow near the downstream part of the second guide vane even changes its direction from counter-rotating to co-rotating with the flows in the main and the third (S_3) passages. This qualitative switch of flow pattern represents an undesired feature from the perspective of fuel atomization.[14]

In spite of the modification of the flowfield between the first and second guide vanes at $f_F=13\,000$ Hz, the distribution of the turbulent kinetic energy appears to be insensitive to external forcing in the bulk of the flowfield. This may be attributed to the weakness of the excitation as compared to the intrinsic high-intensity flow motion. The kinetic energy of the periodic motion is considerably smaller than that of the turbulent motion at the injector outlet. The broadband nature of the injector flow also discourages the modulation of the mean flow by a single-harmonic excitation unless the forcing resonates with the local flow structure at appropriate frequencies.[9]

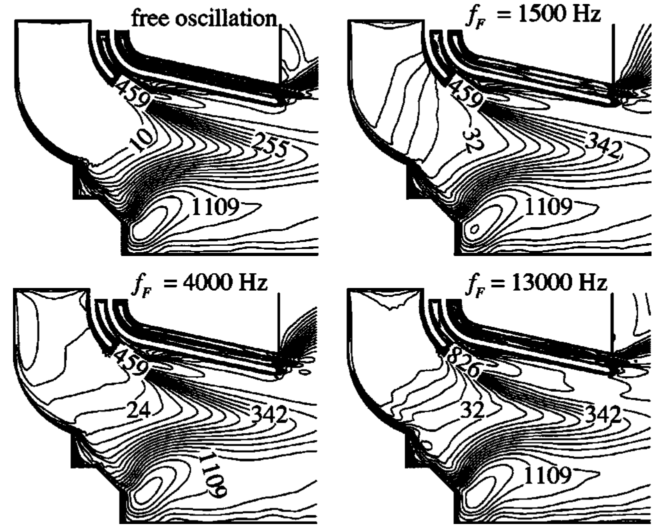

FIG. 11. Effect of external forcing on turbulent kinetic energy. Contour levels between 10 and 3600 m^2/s^2 with exponential distribution.

C. Response of injector flow

The dynamic response of the injector to external excitations was first characterized by conducting an extensive survey of the frequency contents of the flowfield. Figure 12 shows the spectra of pressure oscillations in the forward section of the main flow passage ($x=0.61R_0$, $y=0.78R_0$, and $z=0.03R_0$) under 500, 1500, and 4000 Hz forcing. Here R_0 is the radius of the injector exit. A dominant harmonic corresponding to the forcing frequency is clearly observed. The

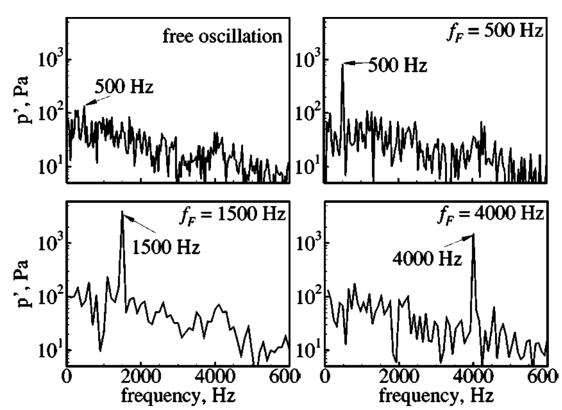

FIG. 12. Frequency spectra of pressure oscillations at $x=0.61R_0$, $y=0.78R_0$, and $z=0.03R_0$ under conditions with and without external excitations.

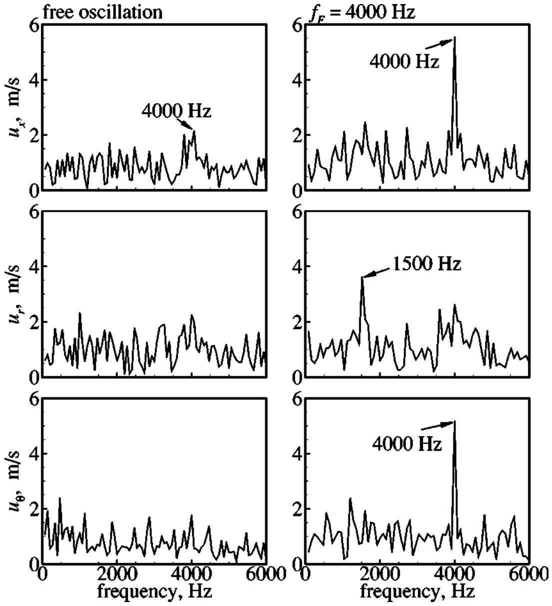

FIG. 13. Frequency spectra of velocity oscillations at $x=1.29R_0$, $y=0.61R_0$, and $z=0.02R_0$ under conditions with and without external excitations.

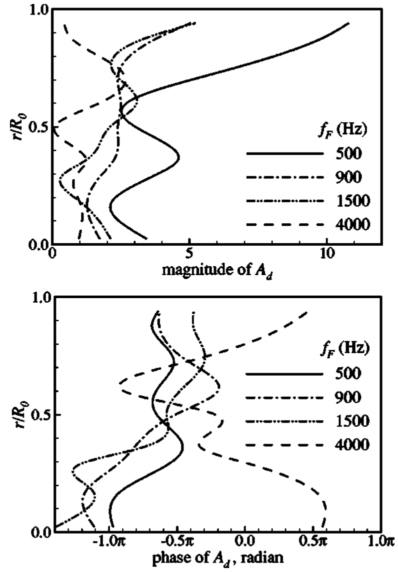

FIG. 14. Radial distributions of acoustic admittance function at injector exit for different forcing frequencies.

excitation at $f_F=1500$ Hz leads to the maximum pressure oscillation among the three cases considered herein.

The velocity field appears not to be as sensitive as the pressure field to external forcing, especially in regions with high turbulence intensity, such as the central recirculation zone and the downstream regions of the guide vanes.[15] Figure 13 shows the frequency spectra of the velocity components at a probe in the main flow passage ($x=1.29R_0$, $y=0.61R_0$, and $z=0.02R_0$) at a forcing frequency of 4000 Hz. The responses are much smaller than that of the pressure, and the axial and azimuthal oscillating magnitudes are higher than the radial counterpart. In the main flow passage, the streamwise and azimuthal velocity fields always exhibit stronger responses due to the impressed oscillations in these two directions at the injector entrance. Conservation of mass and angular momentum, along with the geometric compactness of the injector in reference to the wavelength of the external forcing, tends to preserve streamwise and azimuthal velocity fluctuations without much diffraction into other spatial directions. At the injector exit, the streamwise oscillation dominates the fluctuating velocity field. The azimuthal velocity oscillation is relatively easily diffused by high-intensity turbulent motion, and then dissipated by viscous effects. Such damping mechanisms have less influence on the pressure oscillation propagating in the form of acoustic wave, and thus result in different responses for the pressure and velocity fields. A related observation of the acoustic and vortical flow evolution is given in Ref. 5.

1. Admittance function

The global response of the injector can be described by the acoustic admittance at the exit. The information obtained can be effectively used to serve as the upstream boundary condition for analyzing the unsteady flow motion in a combustion chamber.[16] The admittance function, also the reciprocal of the impedance function, measures the velocity fluctuation in response to incident pressure fluctuation. Following common practice, the acoustic admittance function, A_d, is defined as

$$A_d(f) = \frac{\hat{u}^a/\bar{a}}{\hat{p}^a/\gamma\bar{p}}, \tag{14}$$

where $\bar{p}$ and $\bar{a}$ denote the mean pressure and the speed of sound, respectively. The caret $(\hat{\ })^a$ represents the Fourier component of the oscillation at the forcing frequency. Since the background noise in the free-forcing case is too strong to obtain meaningful results, an external excitation is required to determine the acoustic admittance at the frequency of concern.

Figure 14 shows the radial distributions of the admittance functions at the injector exit for four different forcing frequencies of 500, 900, 1500, and 4000 Hz. The maximum response occurs at 500 Hz, especially near the rim of the second guide vane. Excitations at 500, 900, and 1500 Hz exhibit the same trend and the admittances achieve their maxima when the outer boundary $r=R_0$ is approached. This may be attributed to the relatively low pressure oscillation and high velocity fluctuations near the upper boundary. In this region, the pressure response at 500 Hz forcing is less than 300 Pa, which is smaller than its counterparts at other excitation frequencies (>1000 Pa). When the oscillation is impressed at 4000 Hz, the velocity response in the outer region ($0.8<r/R_0<1.0$) becomes very small. Since the liquid film breaks up in the trailing edge of the second guide vane, the flow response in this region plays an important role in dictating the dynamic behavior of the liquid fuel.[6] A small pressure oscillation at 500 Hz may result in a large velocity fluctuation, which consequently exerts a strong influence on spray formation at that location.

The phase distribution of the admittance function indicates a lag between the velocity and pressure fluctuations

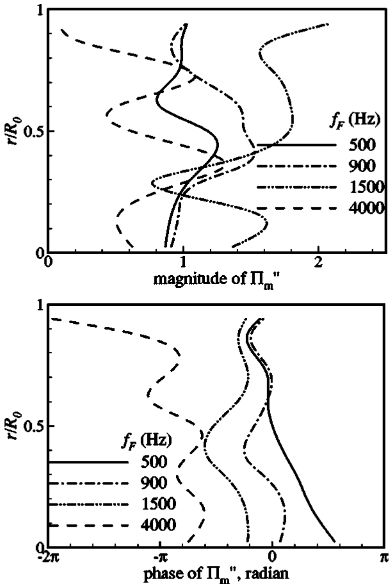

FIG. 15. Radial distributions of transfer function of mass flux at injector exit for different forcing frequencies.

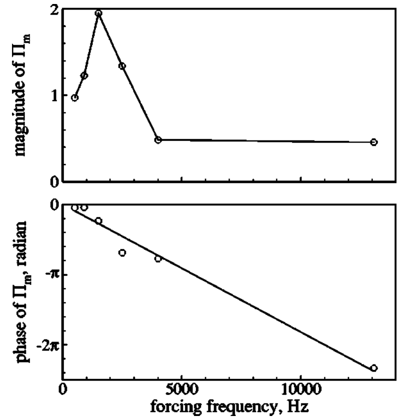

FIG. 16. Effect of forcing frequency on transfer function of total mass flow rate.

around 90° in the main flow passage $(0.3<r/R_0<0.8)$. The situation is consistent with the behavior of a simple traveling acoustic wave without much influence from shear layers. The phase behavior for the 4000 Hz case exhibits a trend distinct from the other cases, especially in the central recirculation zone. A major factor contributing to this phenomenon is the proximity of this forcing frequency to the characteristic frequency of the central recirculating flow.[1] The imposed axisymmetric excitation in the streamwise and azimuthal directions does not promote the evolution of the precessing vortex along the boundary of the central recirculation zone. The pressure and velocity coupling at 4000 Hz is different from that at other frequencies because of the phase difference between the oscillations induced by external forcing and intrinsic flow instabilities.

2. Mass transfer function

Another important measure of the injector dynamic response is the mass-flux transfer function, defined as follows:

$$\Pi_m''(f) = \frac{\widehat{\dot{m}}_{\mathrm{ex}}''^{\,a} A_{\mathrm{ex}}}{\widehat{\dot{m}}_{\mathrm{in}}''^{\,a} A_{\mathrm{in}}}, \tag{15}$$

where $\dot{m}''^a$ represents the Fourier component of the mass flux at the forcing frequency and A the cross section area. The subscripts in and ex denote the injector entrance and exit, respectively. The mass flux oscillation at the entrance, $\widehat{\dot{m}}_{\mathrm{in}}''^{\,a}$, remains constant, since the magnitude of the mass flow oscillation is fixed at 10% as an inlet flow condition. Figure 15 shows the radial distributions of the transfer functions for four different forcing frequencies. The mass flux at the exit is significantly modulated by the external excitation. The magnitude distribution is almost uniform in the range of 1 ± 0.2 under low-frequency forcing at 500 and 900 Hz. The magnitude for $f_F=1500$ Hz, however, is greater than two near the upper boundary, where the flow characteristic frequency is in the range of 1200–1800 Hz.[1] It decreases to less than unity near the boundary of the central recirculation zone, $r/R_0 \sim 0.3$. The excitation may resonate with the flow motion in the main flow passage in a form of shedding ring structures, as shown in Fig. 8, and considerably modifies the local flow evolution. In a striking contrast, the influence of the 4000 Hz forcing is much reduced. In spite of the existence of a peak near the boundary of the central recirculation zone $(\sim 0.3r/R_0)$, where the natural frequency is around 4000 Hz,[1] the response within the central recirculating flow and the downstream regions of the guide vanes remains weak. This observation is consistent with the result of the acoustic admittance function discussed earlier. The 4000 Hz external excitation only exerts a minor influence on the precessing motion of the central recirculating flow. Gallaire *et al.*[10] also observed a similar phenomenon, in which vortex breakdown was mainly controlled by the dynamics in the core region near the centerline, not so much by the excitation in the main flow passage surrounding the central recirculation zone.

The instantaneous distribution of mass-flux fluctuation depends greatly on the forcing frequency, although the profile of the mean mass flux is almost identical to each other. The ensuing effect on the air/fuel distribution and mixing in an operational injector could be significant. The overall behavior can be characterized using the transfer function of the total mass flow rate between the injector entrance and exit, defined as

$$\Pi_m(f) = \frac{\widehat{\dot{m}}_{\mathrm{ex}}^{a}}{\widehat{\dot{m}}_{\mathrm{in}}^{a}}. \tag{16}$$

Here $\widehat{\dot{m}}^a$ is the Fourier component of the mass flow rate at the forcing frequency, which is obtained by integrating the mass flux over the entire surface of concern. Figure 16 shows the magnitude and phase of Π_m as a function of the forcing frequency. The magnitude reaches its maximum at $f_F=1500$ Hz, as expected from the previous results. A large disparity of the fluctuation of the mass flow rate between the entrance and exit is clearly found. This observation, at a first glance, seems to violate the law of mass conservation for such an acoustically compact injector, for which the forcing

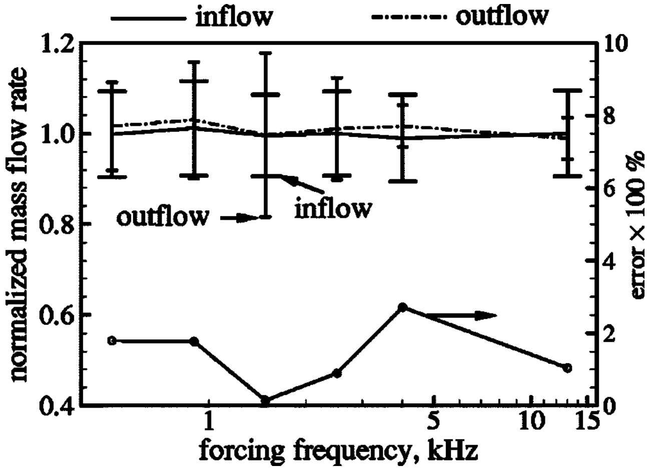

FIG. 17. Mean total mass flow rates and magnitudes of Fourier components of mass flow rate for different excitation frequencies.

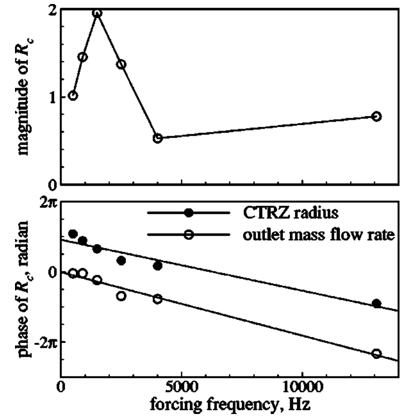

FIG. 18. Effect of forcing frequency on fluctuation of normalized CTRZ radius.

frequency is much lower than the acoustic characteristic frequency of the injector, f_a. Under this condition, the flowfield in the injector can be treated as incompressible, and the instantaneous total mass flow rate at the entrance and exit should be identical. To explore the underlying physical mechanisms responsible for the phenomenon shown in Fig. 16 and to ensure numerical accuracy, the time-averaged mass flow rates at the injector entrance and exit are calculated. The result shown in Fig. 17 for a sampling period of two cycles of oscillation confirms the conservation of the overall mass flow rate for all the forcing frequencies considered herein. The maximum difference of 2.6% may result from numerical errors. Also included in Fig. 17 is the excursions of the instantaneous mass flow rates at the two ends of the injector. The 1500 Hz forcing indeed excites the flowfield at the expense of suppressing fluctuations at the other frequencies. The mass-flow transfer function for the 4000 Hz forcing is less than unity. In addition to the channeling of mass flow among different Fourier components, flow compressibility takes effect at high-frequency forcing, allowing for a relatively large mass variation inside the injector temporarily. In short, the forcing frequency affects not only the spatial distribution of the mass flux fluctuation, but also the temporal variation of the overall mass flow rate.

The phase shift in Fig. 16 exhibits a linear distribution with the forcing frequency due to compressibility effects. This phenomenon can be examined using the acoustic characteristic frequency, f_a, and the phase difference, θ, in Eq. (13). The good agreement between the analytic estimation, Eq. (13), and the numerical result further verifies that the oscillation of the mass flow rate propagates in the form of acoustic wave.

3. Radius of central recirculation zone

In view of the importance of the central recirculation zone in a swirling flow, it is instructive to investigate its dynamic response to external excitations. A dividing streamline is used to define the boundary of the central recirculation zone, whose radius, r_c, at the injector exit is determined through the following definition:

$$\dot{m}(r_c) = 2\pi \int_0^{r_c} \widehat{\widehat{\rho u}}_x r dr = 0, \tag{17}$$

where $(\frown)$ represents the spatial averaging in the azimuthal direction. The net mass flow rate in the region between the centerline and r_c is zero. The periodic variation of the radius of the dividing streamline is further normalized with its mean value,

$$R_c(f) = \frac{\hat{r}_c^a / \overline{r_c}}{\widehat{\dot{m}}_{\mathrm{in}}^a / \overline{\dot{m}}_{\mathrm{in}}}, \tag{18}$$

where R_c denotes the Fourier component of the normalized radius at the forcing frequency. The phase of the normalized radius, shown in Fig. 18, lags that of the mass flow rate by 180°. The external excitation affects not only the mass flux magnitude, but also the effective passage area. The detailed flow evolution within one cycle of oscillation at the 1500 Hz forcing is shown in Fig. 19, where the flowfield is spatially averaged in the azimuthal direction. The size of the central recirculation zone shrinks to a minimum when the mass flow rate reaches its maximum at the exit, and vice versa. This phenomenon suggests that the magnitude of the mass-flow-rate oscillation can exceed that of the mass-flux fluctuation, due to the modulation of the central recirculating flow.

The above phenomenon seems to conflict with the result of the spectral analysis presented earlier, in which no observation is made of strong velocity response near the boundary of the central recirculation zone at the 1500 Hz forcing. The visualization result shown in Fig. 19 is attributed to the reduced-order data analysis implemented in the present study. The turbulent swirling flow is fully three-dimensional and features strong helical motion, large-scale intermittence, and high background noise, as shown in Fig. 1. Thus the spectral information at a single point may misrepresent dominant flow mechanisms. The spatial averaging in the azimuthal direction effectively filters out the influences of helical motion and the background noise, and hence improves the understanding of key phenomena in a complex flowfield.

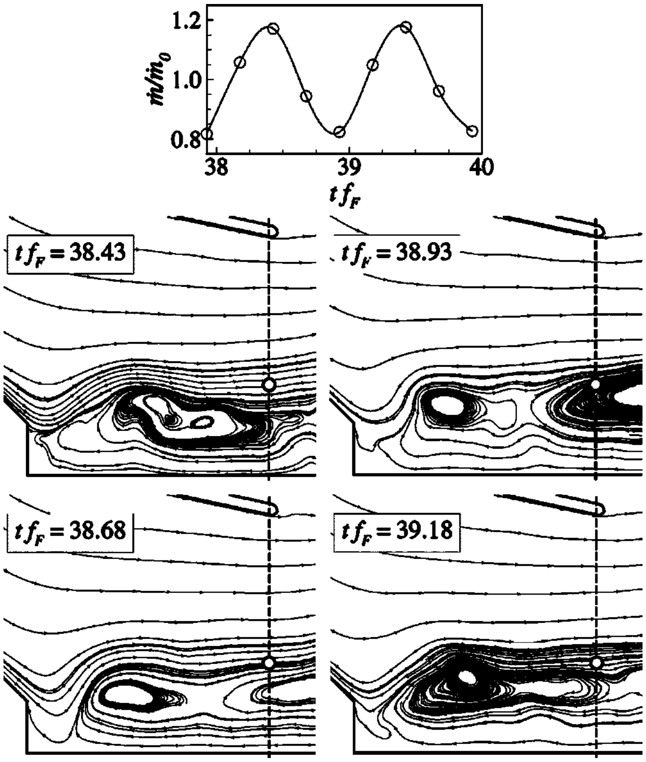

FIG. 19. Time evolution of streamlines within one cycle of oscillation for forcing frequency of 1500 Hz, spatially averaged in azimuthal direction. The open circle on the dashed line denotes long-time averaged CTRZ radius.

IV. CONCLUSIONS

A comprehensive numerical analysis based on a large-eddy-simulation (LES) technique has been conducted to investigate the internal flow evolution and dynamic response of a swirl injector under external forcing over a broad range of frequencies. The excitation was imposed by periodically varying the mass flow rate at the injector entrance. Results indicate that the impressed disturbance can be decomposed into two parts propagating at different velocities. The flow oscillation in the streamwise direction propagates in the form of acoustic wave at the speed of sound, whereas its azimuthal counterpart is convected with the local flow, according to the conservation of mass and angular momentum. An important observation is that the imposed axisymmetric excitation does not exert much influence on the evolution of the central recirculating flow, even when the forcing frequency is identical to the characteristic frequency of the vortex precession around the recirculation zone. The flowfield in that region is mainly controlled by the dynamics in the vortex core near the centerline, not so much by the excitation in the main flow passage surrounding the central recirculation zone. Because of the broadband nature of the injector flowfield, the effects of external forcing on the mean flow properties appear to be quite small, except in regions where the characteristic frequencies of the flow motion match the forcing frequency. The flow evolution under forcing is highly frequency-dependent. Low-frequency excitations in general promote flow fluctuations, but the trend is reversed for high-frequency excitations. The global response of the injector is characterized using the acoustic admittance and mass transfer functions. The fluctuation of the instantaneous mass flow rate of a given frequency component at the injector exit may reach a magnitude substantially greater than that at the entrance when the forcing resonates with the injector flow.

ACKNOWLEDGMENTS

This work was sponsored by the NASA Glenn Research Center under Grant No. NAG 3-2151. Kevin Breisacher was the Contract Monitor. The authors are grateful for technical discussions with Dr. Jeff Cohen of United Technologies Research Center.

[1]S. Wang, S. Hsieh, and V. Yang, "Unsteady flow evolution in swirl injector with radial entry. I. Stationary conditions," Phys. Fluids **17**, 045106 (2005).
[2]C.-M. Ho and P. Huerre, "Perturbed free shear layers," Annu. Rev. Fluid Mech. **16**, 365 (1984).
[3]J. Panda and D. McLaughlin, "Experiments on the instabilities of a swirling jet," Phys. Fluids **6**, 263 (1994).
[4]L. Cerecedo, L. Aisa, J. Garcia, and J. Santolaya, "Changes in a coflowing jet structure caused by acoustic forcing," Exp. Fluids **36**, 867 (2004).
[5]S. Apte and V. Yang, "Unsteady flow evolution in porous chamber with surface mass injection, 2. Acoustic excitation," AIAA J. **40**, 244 (2002).
[6]J. Cohen and J. Hibshman, "An experimental study of combustor air swirler acoustic and fluid dynamic sensitivities," in Propulsion Engineering Research Center Ninth Symposium on Propulsion, Cleveland, OH, 1–2 October 1997.
[7]C. Paschereit, E. Gutmark, and W. Weisenstein, "Coherent structures in swirling flows and their role in acoustic combustion control," Phys. Fluids **11**, 2667 (1999).
[8]T. Lieuwen and Y. Neumeier, "Nonlinear pressure-heat release transfer function measurements in a premixed combustor," Proc. Combust. Inst. **29**, 99 (2002).
[9]G. Brereton, W. Reynolds, and R. Jayaraman, "Response of a turbulent boundary layer to sinusoidal free-stream unsteadiness," J. Fluid Mech. **221**, 131 (1990).
[10]F. Gallaire, S. Rott, and J.-M. Chomaz, "Experimental study of a free and forced swirling jet," Phys. Fluids **16**, 2907 (2004).
[11]A. Hussain and W. Reynolds, "The mechanics of organized wave in turbulent shear flow," J. Fluid Mech. **41**, 241 (1970).
[12]Y. Huang, "Modeling and simulation of combustion dynamics in lean-premixed swirl-stabilized gas-turbine engines," Ph.D. thesis, Pennsylvania State University, University Park, PA, 2003.
[13]J. Lasheras and E. Hopfinger, "Liquid jet instability and atomization in a coaxial gas stream," Annu. Rev. Fluid Mech. **32**, 275 (2000).
[14]J. Chin, N. Rizk, and M. Razdan, "Effect of inner and outer airflow characteristics on high liquid pressure prefilming airblast atomization," J. Propul. Power **16**, 297 (2000).
[15]S. Wang, "Vortical flow dynamics and acoustic response of gas-turbine swirl-stabilized injectors," Ph.D. thesis, Pennsylvania State University, University Park, PA, 2002.
[16]F. Culick and V. Yang, "Overview of combustion instabilities in liquid propellant rocket engines," in *Liquid Rocket Engine Combustion Instability*, Vol. 169, edited by V. Yang and W. Anderson, Progress in Aeronautics and Astronautics 1 (AIAA, Reston, VA, 1995), Chap. 1, pp. 3–37.